RSC Advances

PAPER

View Article Online
View Journal | View Issue

Cite this: *RSC Adv.*, 2026, **16**, 18270

Photothermal-responsive self-healing PDMS-based elastomers for stretchable strain sensors

Ruijie Zhu,[ab] Ling Ai,[*bc] Zhou Zhou,[b] Jie Gao,[b] Yuanlong Zhong,[b] Qi Zhang[b] and Weijie Song[*bcd]

The modification of traditional self-healing elastomers is typically accompanied by a loss of both strength and self-healing efficiency, limiting their long-term reliability. Developing multifunctional polydimethylsiloxane (PDMS)-based systems capable of overcoming this trade-off is thus critical for practical sensor applications. In this work, a photothermal-responsive self-healing PDMS elastomer (PUSE) was designed by constructing an elastomeric network from PDMS and isophorone diisocyanate (IPDI), with 4, 4′-dithiobisdiphenylamine (APDS) and epoxy-functionalized 2, 4, 6, 8 -tetramethyl – 2, 4, 6, 8 – tetra [3 – (hydroxyphenylmethoxy) propyl] cyclotetrasiloxane (TEC) as chain extenders. The synergistic effect of dynamic disulfide bonds and hydrogen bonds endowed the elastomer with reversible self-healing ability, while rigid phenyl and siloxane rings enhanced mechanical robustness. The optimized PUS_3E elastomer exhibited a tensile strength of 4.2 MPa, a toughness of 9.85 MJ m^{-3}, and a resilience of 364.70%, Moreover, the self-healing efficiency reached 94.76% under UV irradiation within 24 h, surpassing 74.90% achieved at 70 °C, demonstrating the effectiveness of photo-thermal-assisted healing. The elastomer also showed hydrophobicity (water contact angle >100°) and optical transparency (T_{550nm} = 87.5%). PUS_3E was also utilized as the substrate for preparing resistive strain sensors that can accurately detect signals from the natural movements of the human body, making them highly valuable in the field of flexible sensors.

Received 19th February 2026
Accepted 19th March 2026

DOI: 10.1039/d6ra01474g

rsc.li/rsc-advances

1 Introduction

With the rapid development of biomedical science and artificial intelligence, wearable electronic devices have attracted extensive attention in the field of sensors,[1,2] soft robots[3,4] and flexible electronic devices.[5,6] Unlike traditional rigid materials, flexible polymer elastomers possess unique characteristics and are of great importance for the new generation sustainable electronics typically including flexibility, shape reconfigurability, and skin compatibility, making them ideal substrates for constructing wearable electronic devices. Elastomers derived from polydimethylsiloxane (PDMS),[7] polyurethane (PU),[8] and hydrogels[9] are widely explored as the main polymer network. Among these, PDMS elastomers with exceptional flexibility, biocompatibility, processability, and thermal stability have shown great potential in wearable electronic devices.[10–12] However, devices inevitably suffer from mechanical deformation and damage caused by repeated friction and bending/folding, giving rise to degraded performance or even failure in multiple scenarios.[13,14] An effective strategy to enhance the mechanical durability of these sensors is to design tough and self-healing elastomers that endow the polymer structure with reversibility feature, stimulating the materials with the mechanical stability and recyclability to extend their service life and improve their reliability.[15–17]

Researchers have designed and prepared various self-healing polysiloxane elastomers by introducing reversible dynamic covalent bonds, such as disulfide bonds,[18–20] imine bonds,[21–23] and metal coordination bonds,[24–26] as well as reversible dynamic non-covalent interactions like hydrogen bonds,[27–29] π–π stacking,[30,31] and van der Waals forces,[32] most of which can be stimulated by heat. For example, Kim *et al.*[33] incorporated reversible oxime–urethane bonds into an elastomer network based on PDMS and isophorone diisocyanate (IPDI) to promote self-healing *via* thermal response. This elastomer exhibited a self-healing efficiency of 93.7% after heating for 6 hours at 65 °C, showing tensile strength of 1.2 MPa. Moreover,[34] room temperature-response PDMS elastomers composed of disulfide dithioesters (DPTA) and aluminum ions (Al^{3+}) were designed, demonstrating a self-healing efficiency up to 97% after 48 hours of reversible facture and reformation from disulfide and metal coordination bonds, with tensile strength of 1.4 MPa. Zhang

[a]*School of Materials Science and Engineering, Jiangxi University of Science and Technology, Ganzhou 341000, Jiangxi, China*

[b]*Laboratory of Optoelectronic Materials and Devices, Ningbo Institute of Materials Technology and Engineering, Chinese Academy of Sciences, Ningbo, 315201, People's Republic of China. E-mail: ailing@nimte.ac.cn; weijiesong@nimte.ac.cn*

[c]*University of Chinese Academy of Sciences, Beijing, 100049, People's Republic of China*

[d]*Jiangsu Collaborative Innovation Center of Photovoltaic Science and Engineering, Changzhou, 213164, People's Republic of China*

et al.[20] constructed a high tensile strength (6.44 MPa), high toughness (37 MJ m^{-3}), and excellent self-healing performance (86% at 80 °C) supramolecular polydimethylsiloxane (PDMS) elastomer network containing hydrazine groups and aromatic disulfide bonds. Liu *et al.*[35] introduced π–π stacking and multiple hydrogen bonds into polysiloxane elastomers, the elastomer exhibited excellent mechanical properties with a tensile strength of up to 7.46 MPa, and its self-healing efficiency reached 96% at 110 °C. To further adjust the self-healing ability and mechanical strength, researchers have proposed a novel strategy involving optical-stimuli materials into the thermal-response polymer networks to achieve synergistic photothermal-assisted self-healing. Most of the as-reported light-response elastomers were obtained by grafting/crosslinking photocurable molecules. For instance, derivatives of azobenzene,[36] CNTs,[37] coumarin,[38] anthracene,[39] and epoxides[40] have been introduced as photoresponsive components. Peng *et al.*[41] utilized azobenzene to induce *cis–trans* isomerization under UV light, thereby constructing a light-responsive polysiloxane elastomer. After UV light exposure, the self-healing efficiency of the elastomer was increased to 95% after 1.8 hours. Fan *et al.*[42] incorporated carbon nanotubes (CNTs) into a PDMS elastomer, achieving rapid self-healing through photothermal conversion. The self-healing efficiency was close to 100% within 40 seconds despite sacrificing toughness. Obviously, the incorporation of photo-response units above leads to a mechanical degradation effect, the multiple covalent crosslinked networks may weaken the original hydrogen bonding, thereby generating conflict between self-healing efficiency and mechanical performance. Therefore, it is still a long-term challenge to break the tradeoff aforementioned, and construct various elastomers to achieve high strength and toughness with self-healing capacity, favorable for the subsequent flexible electronic devices.

For elastomeric systems based on silicone polymers, epoxy-functionalized silicones can form a crosslinked network through both ultraviolet (UV) and thermal curing methods.[43] Zhao *et al.*[44] synthesized an elastomer capable of self-healing at room temperature (12 hours, 91%, the tensile strength is 0.5 MPa) using diglycidyl ether-terminated PDMS and diphenyl disulfide. However, silicone polymers functionalized with epoxides, lactones and poly(organosiloxane) bearing cyclic ether functionalities can also undergo cationic polymerization under UV light exposure. In particular, epoxy-functionalized organosilicon polymers can further improve mechanical properties and thermal stability. For example, Zhao *et al.* synthesized a glycidyl epoxide-terminated polysiloxane, based on hydride-terminated polysiloxane, using the Karstedt catalyst.[45] In this work, we selected 2,4,6,8-tetramethyl-2,4,6,8-tetrakis [3-(oxiranylmethoxy) propyl] cyclotetrasiloxane (TEC) with epoxy-functionalized terminal groups as the light-response unit, in combination with an intrinsic self-healing network to achieve opto-thermal-response sensor with reliable dynamic sensing performance. The main chain of the elastomer PUSE was constructed by using polydimethylsiloxane (PDMS) and isophorone diisocyanate (IPDI), with 4,4′-dithiodiphenylamine (APDS) and 2,4,6,8-tetramethyl-2,4,6,8-tetrakis [3-(oxiranylmethoxy)propyl] cyclotetrasiloxane (TEC) serving as chain extenders. Disulfide bonds and epoxy groups were introduced to enhance the self-healing efficiency (the self-healing efficiency under UV light is 94.76%, which is superior to 74.90% at 70 °C), while benzene rings and siloxane rings were incorporated to improve the mechanical properties (the tensile strength was improved from 2.19 MPa to 4.20 MPa). By adjusting the composition, both the mechanical properties and self-healing performance of the PUSE elastomer were synergistically enhanced. To construct a wearable stress–strain sensor based on PUSE, Ag nanowires (AgNWs) were incorporated with the PUSE elastomer using a transfer method. The PUSE/AgNWs composite elastomer film was successfully fabricated and applied for real-time monitoring of human motion, demonstrating promising development prospects and application value in the field of flexible wearable sensors.

2 Result and discussion

2.1. Molecular design and characterization of the elastomer

In order to obtain elastomeric materials that combine mechanical strength and self-healing capabilities, the PUSE polymer was synthesized *via* a two-step condensation reaction (the synthetic routes are shown in Fig. S1). Fig. 1a illustrates the molecular design of PUSE. Aminopropyl-terminated polydimethylsiloxane (PDMS) and isophorone diisocyanate (IPDI) were selected as the soft and hard segments, respectively extender. To construct a photo-thermal synergistic self-healing elastomer network, 2, 4, 6, 8 – tetramethyl – 2, 4, 6, 8 – tetrakis [3 – (oxiranylmethoxy) propyl] cyclotetrasiloxane (TEC) with dual crosslinkable function was introduced as a UV-responsive molecule. The four-terminal epoxy groups on TEC can react through epoxy ring-opening self-polymerization induced by photoinitiator, along with hydrogen bonding between the residue hydroxy group from ring-opening process and the main chain. It is worth noting that the formation of dimensional network from crosslinked tetrasiloxane units also presented as hard segments due to the inner-molecular steric-hindrance effect, enabling the target elastomer with intensified roughness and controllable stress. Fig. 1b illustrates the bonding generated between and within the molecular chains in the PUSE elastomer network. The target PUSE elastomer composed of multi-crosslinked chains contains a abundant of dynamic sacrifice bonds, including disulfide bonds as dynamic reversible covalent bonds, along with strong and weak hydrogen bonds as dynamic reversible non-covalent bonds, endowing target composites with promoted mechanical performance and self-healing capabilities under the synergistic effect *via* both thermal and light response segments.

Fig. 2a shows the FTIR spectra of IPDI, H_2N-PDMS-NH_2, TEC, PU, and PUSE. The absorption peak at 3345 cm^{-1} corresponds to the stretching vibration of the N–H bond was observed. The absorption peak at 2247 cm^{-1} was attributed to the asymmetric stretching vibration of the –NCO group. The attenuated absorption peak of N–H bond revealed that the amino groups from H_2N-PDMS-NH_2 successfully reacted with the isocyanate groups in IPDI. The peak at 3500 cm^{-1} corresponds to the

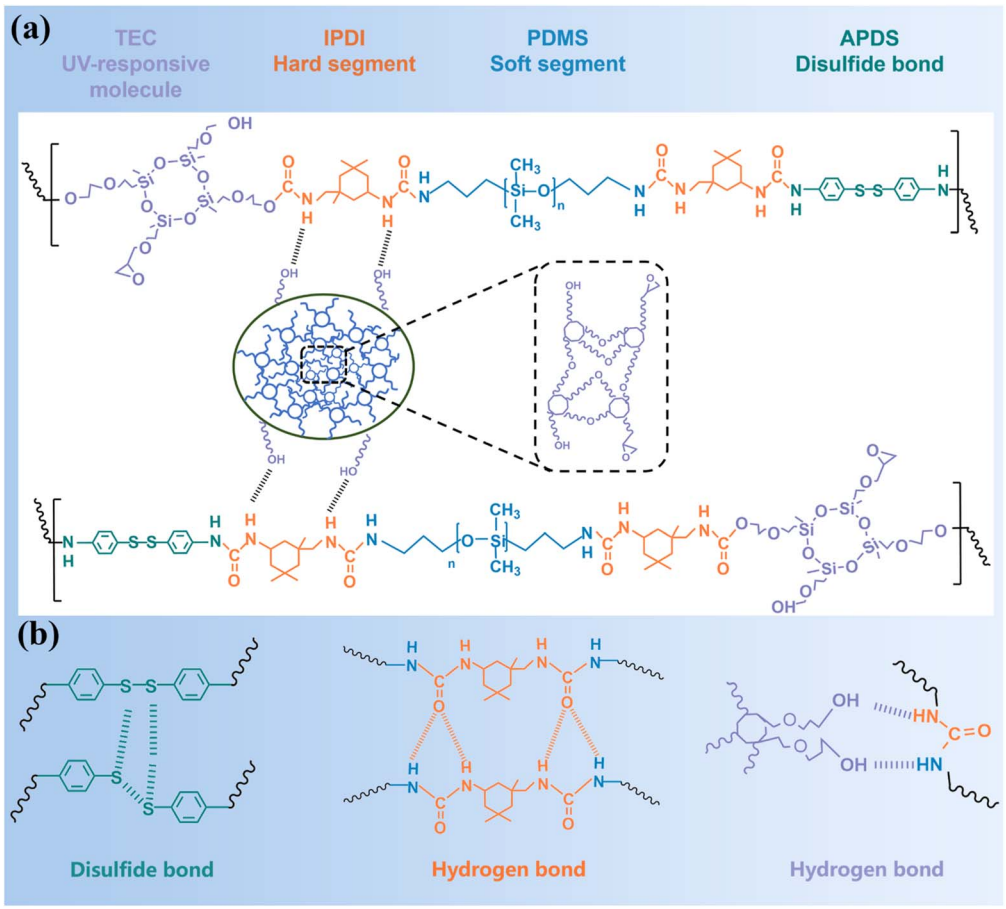

Fig. 1 (a) Molecular design of PUSE. (b) Bonds between and within the molecular chains in the PUSE elastomer network.

stretching vibration of the O–H bond, which formed *via* the ring-opening reaction of epoxy groups in TEC under UV light. Compared to PU, the –OH groups in TEC can react with the excess –NCO groups to form amide ester bonds, and the disappearance of the asymmetric stretching vibration peak of –NCO in PUE proved the complete reaction of IPDI. The absorption peak at 906 cm^{-1} was the characteristic peak for the stretching vibration of the –C–O–C– bond. The disappearance of

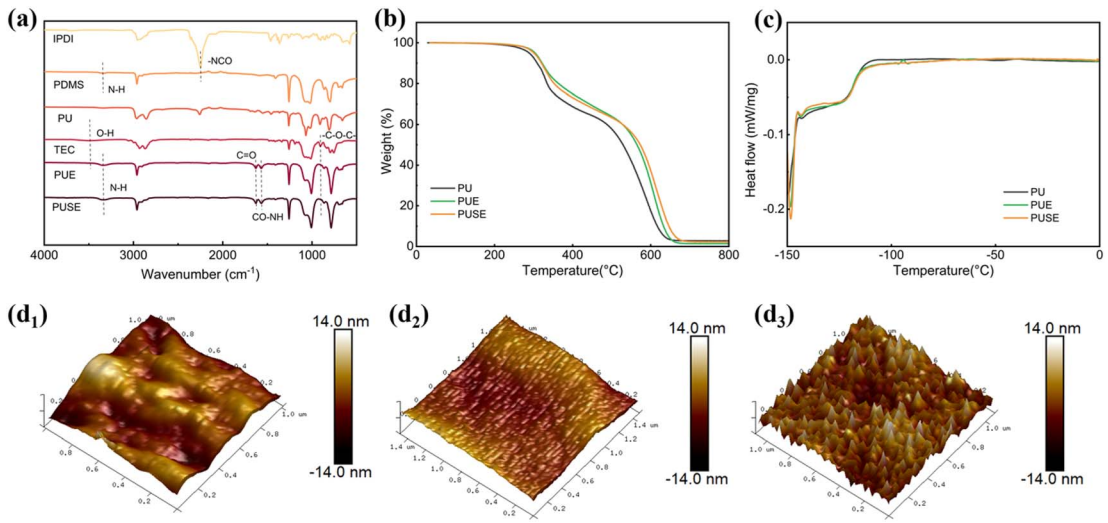

Fig. 2 (a) The infrared spectra of IPDI, H_2N-PDMS-NH_2, TEC, PU, PUE, PUSE. (b) PU, PUE, and PUSE elastomers TGA curve. (c) PU, PUE, and PUSE elastomers DSC curve. (d) AFM image of the surface of elastomers (d1: PU, d2: PUE, d3: PUSE).

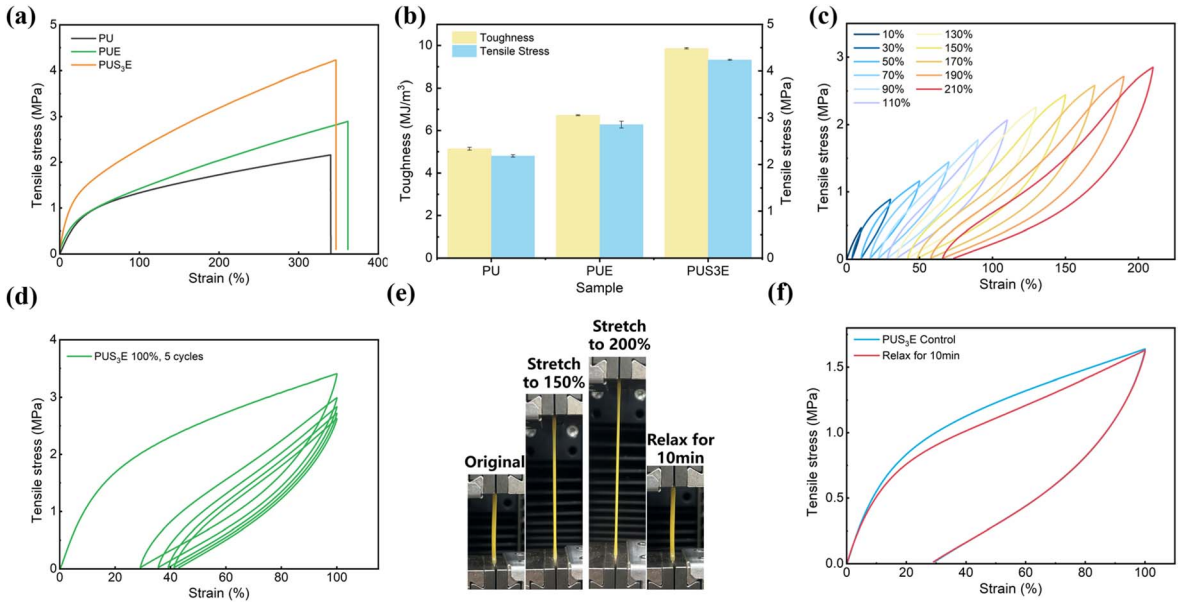

Fig. 3 (a) Stress–strain curves of PU, PUE, PUS_3E. (b) Tensile strength and Toughness of PU, PUE, PUS_3E. (c) Cyclic loading-unloading tensile curves of the PUS_3E elastomer at increasing strain (10–210%). (d) The continuous cyclic tensile curves of the elastomer PUS_3E at 100% strain for five consecutive cycles. (e) Cyclic loading-unloading tensile testing of the PUS_3E elastomer for 5 cycles at 100% strain. (f) Cyclic loading-unloading tensile curve of the PUS_3E elastomer after one cycle at 100% strain and relaxation for 10 minutes.

this peak in PUE suggested the successful incorporation of TEC, along with its epoxy groups fully crosslinked with the polymer main chains. Additionally, new absorption peaks at 1631 cm^{-1} and 1569 cm^{-1} appeared in PUE, corresponding to the stretching vibrations of C═O and CO–NH, further confirming the presence of the urea structure in PUE. Fig. S2 also shows the Raman response curves of PU, PUE, and PUSE in the range of 400 cm^{-1} to 500 cm^{-1}. The Raman response peak of Si–O–Si at 492 cm^{-1} overlaped with the S–S peak, and since the Raman response of Si–O–Si was stronger than that of S–S, the S–S peak was covered.[46] The spectra shown in Fig. S3 demonstrated that the successful synthesis of the PUSE polymer.[47,48] In the X-ray photoelectron spectroscopy (XPS) of PUSE, the S 2p peak at 160 eV can be observed, confirming the successful incorporation of S–S bonds into PUSE[49,50] (Fig. S4).

Thermal properties of elastomers were evaluated by TGA and DSC, as displayed in Fig. 2b and c. The initial decomposition temperature (T_d: the thermal decomposition temperature with a 5% mass loss) of the TEC-modified PUE elastomer is 303.66 °C, which is higher than that of the unmodified PU (288.60 °C). TEC contains both Si–O bonds and octagonal ring structures endows PUE with good heat-resistance, strengthening the rigidity of the network and restricting the movement of the molecular chains. Therefore, the incorporation of TEC improves the thermal stability of the elastomer. However, after the embedding of APDS, the T_d of PUSE decreased to 300.48 °C, slightly lower than that of PUE. On the one hand, the introduction of aromatic ring structures in the PUSE system might reduce the crosslink degree of the system due to large steric hindrance from aromatic rings; for another, S–S bonds are less stable than C–C and Si–O bonds and they tend to break at high temperature, which may negatively affect the thermal stability of target PUSE. Despite the slight decrease in thermal stability compared to PUE, the T_d of PUSE is still above 300 °C, higher than that of PU. Therefore, both PUSE and PUE exhibit excellent thermal stability. Fig. 2c also shows the differential scanning calorimetry (DSC) curves of PU, PUE, and PUSE elastomers. The glass transition temperatures (T_g) of PU, PUE, and PUSE are −117.2 °C, −117.5 °C, and −117.2 °C, respectively. Due to the relatively large molecular weight of PDMS and the fact that TEC and APDS are introduced only in small amounts, their influence on the mobility of the overall polymer chains is minimal. From the AFM images (Fig. 2d), it can be observed that no microphase separation occurs in PU and PUE. After the introduction of TEC, the surface roughness of the elastomer decreased, possibly due to the increased hydrogen bond density within the molecular chains, which enhanced the crosslinking degree of the PUE elastomer network and boosted the formation of a more homogeneous matrix. The introduction of APDS as a rigid segment was speculated to adjust the regularity of the elastomer network. As shown in Fig. 2d, the dark areas represent the soft phase and the bright areas represent the hard phase, indicative of the microphase separation structure of PUSE, thus leading to an increase in roughness.

2.2. Mechanical properties of the elastomer

To analyze the mechanical properties of the elastomer, samples were cut into a dumbbell shape with dimensions of 50 mm in length, 4 mm in width, and 2 mm in thickness for tensile testing, with a tensile speed of 10 mm min^{-1}. First, the stress–strain curves of PUE elastomers with different TEC contents were investigated (Fig. S5a). The results showed that the tensile

strength of the PUE elastomer increased from 2.19 MPa to 2.89 MPa when 1 wt% of TEC was grafted, along with its elongation at break improves from 326% to 361.6%, exhibiting distinct improvement compared to PU main chain (Fig. 3a). The introduction of TEC in the main chain increased the cross-linking degree by strong covalent bonds with urea groups on the linear PU, allowing the cyclic structure of TEC to closely cross-link with the linear structure of PU. However, the stretchability of the material sacrificed when excess TEC units were applied. With the raised TEC content, excess TEC had not effectively form hydrogen bonds with the linear main chain, and the large steric hindrance of the cyclic TEC structure limited the movement of the molecular chains, thereby both the tensile strength and elongation at break of the PUE elastomer decreased. It is supposed that the excess TEC units with four-terminal epoxy groups could also react through epoxy ring-opening self-polymerization under UV light exposure. The obtained PUE elastomer endowed with a higher hydrogen bond density can dissipate more energy from external stretching forces through the breaking of hydrogen bonds compared to the initial PU, thus exhibiting superior mechanical properties. Here, we selected PUE with a TEC content of 1 wt% for further optimization and investigation. In the next step of modification, we selected diphenyl disulfide (APDS) as a rigid segment to incorporate into the PUE network above. Fig. S5b shows the stress–strain curves of the PUSxE elastomers with different molar amounts of APDS. The tensile strength of the elastomer increased apparently, while the elongation at break decreased after the introduction of APDS. The PUS_3E elastomer, with 0.3 mmol of APDS, exhibited superior overall mechanical properties (Fig. 3a and b), with a tensile strength of 4.2 MPa, toughness of 9.85 MJ m^{-3}, and elongation at break of 346.8%. The rigid phenyl rings and covalent disulfide bonds in APDS contributed to the enhancement of the tensile strength. Unfavorably, the rigid segments hinder the migration of polymer chains, thereby affecting the elongation at break of the elastomer. Considering the comprehensive tensile strength and toughness, we selected PUS_3E for subsequent cyclic tensile performance testing.

To evaluate the resilience and durability of the PUS_3E elastomer, the samples were cut into dumbbell-shaped specimens with dimensions of 50 mm in length, 4 mm in width, and 2 mm in thickness for cyclic loading-unloading tests under different strains (10–210%) and constant strain (100%) at a stretching speed of 10 mm min^{-1}. Fig. 3c shows the continuous cyclic tensile tests of PUS_3E elastomer with gradual increasing strains from 10% to 210%, with no interval between two consecutive tensile cycles. The elastomer exhibits a relatively weak hysteresis phenomenon under a 50% smaller strain (Fig. S5c). It can be observed that the overall curve shape remains consistent, and the area of the hysteresis loop increases with the increasing strain, indicating that energy dissipation of the elastomer enhances during the stretching process. It is hypothesized that the energy dissipation is attributed to the increasing break of both weak and strong hydrogen bonds, exhibiting significant hysteresis and strain flexibility behavior. Fig. S6 shows that when PUS_3E was stretched to twice its original length and left to rest for 30 seconds, it almost fully recovered to its original length macroscopically, demonstrating that the elastomer can recover significantly in a short period of time after deformation. As shown in Fig. 3d, further cyclic loading-unloading test was carried on PUS_3E at 100% strain for five consecutive cycles to evaluate its resilience at 100% strain. PUS_3E exhibits 50% residual strain and shows significant hysteresis in the first cycle, with a noticeable reduction in the area of the hysteresis loop in cycles 2 to 5. This behavior may be due to the incomplete recovery of cracked dynamic bonds in the first cycle. After being relaxed at room temperature for five minutes, the elastomer regained some of its elasticity, as shown in Fig. S5d. After 10 minutes of relaxation at room temperature. The loading-unloading curve overlaps with the first cycle curve, and the PUS_3E elastomer recovers to its initial state (Fig. 3e and f), elucidating that the reversible dissociation/recombination of dynamic bonds endow PUS_3E with fast healing property as well as significant resilience. The excellent resilience can be attributed to several factors: first, energy dissipation occurs due to the entanglement of polymer chains during the stretching process; second, the reversible dissociation/recombination of hydrogen bonds during deformation; and third, covalent cross-linking ensures structure stability. The broken hydrogen bonds can rebind upon stress release, while the flexible chain segments gradually return to their original state under chain migration, thereby imparting excellent resilience and fatigue resistance to the material.[51]

2.3. Self-healing performance, hydrophobicity, and optical transmittance of the elastomer

The self-healing performance of PUS_3E primarily originated from reversible interaction of dynamic non-covalent hydrogen bonds consisted in both inner- and inter-molecular chains and dynamic covalent disulfide exchange (as illustrated in Fig. 4a). In addition to thermal-driven self-healing bonds, UV light-triggered autonomous self-healing fragments TEC had been incorporated, which were expected to confer self-healing capability under UV-light exposure and accelerate the rearrangement of the dynamic interactions. A scratch with a width of approximately 0.2–0.4 mm was introduced on the surface of the elastomer by using a utility knife, the optical microscope images of the surface scratch self-healing behavior of elastomer films (PU, PUE, and PUS_3E) under UV light exposure for different times were presented in Fig. 4b. In contrast with PU, PUE and PUS_3E exhibited superior self-healing performance mainly due to the incorporation of the UV-responsive molecule TEC. After 50 minutes of UV light exposure, the surface scratches on PUE and PUS_3E films almost disppeared. To further evaluate the self-healing performance of the PUE and PUS_3E elastomers, the samples were cut in half using a utility knife and then rejoined under two conditions (70 °C and UV irradiation for 24 h). Fig. 4c and S7 shows the tensile strength self-healing efficiency of PUE and PUS_3E after 24 h under different conditions. For PUE, the self-healing efficiency under UV irradiation reached 96.89%, which was higher than that efficiency of 93.42% obtained at 70 °C thermal-driven healing for 24 h. Identically for PUS_3E, the

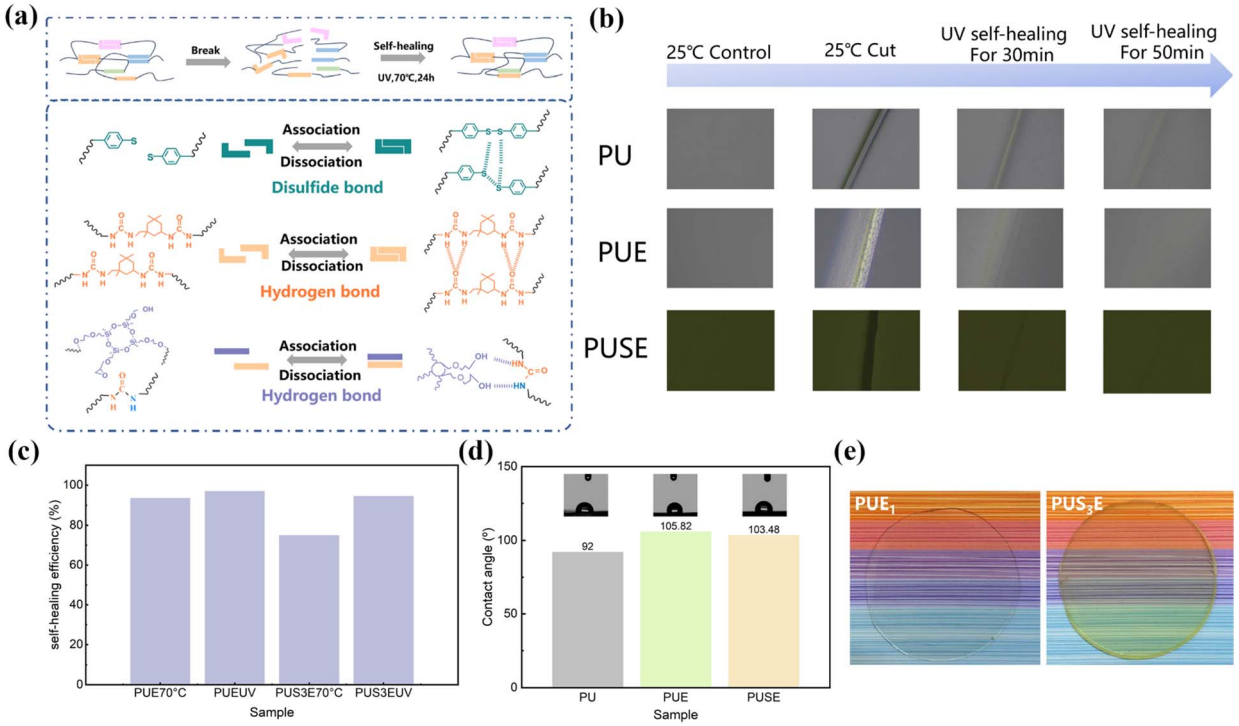

Fig. 4 (a) Schematic illustration of the self-healing mechanism of disulfide bond-containing elastomer. (b) Microscopic images of scratch self-healing in elastomer under UV irradiation for different times. (c) Self-healing efficiency of tensile strength in elastomer after 24 h under different conditions (UV, 70 °C). (d) Water contact angle on the surface of the elastomer. (e) Macroscopic images of the elastomer and its optical transmittance.

efficiency after 24 h of UV irradiation increased from 75.66% (70 °C, 24 h) to 94.76%. According to the results above, it can be concluded that the photothermal self-healing effect assisted by UV irradiation is superior to that of thermal-induced self-healing alone. The mechanism by which this photothermal synergy enhances self-healing performance can be explained as follows: on the one hand, part of the photon energy from UV irradiation is converted into heat, and the elevated temperature facilitates the recombination of dynamic S–S exchanges and reversible hydrogen-bond interactions within the molecular chains, thereby enabling thermally driven self-healing of the elastomer. On the other hand, the TEC units contain numerous unopened epoxy groups that can undergo ring-opening reactions under UV irradiation, generating additional hydrogen bonds and connecting with the main chains. Moreover, UV irradiation can promote the dynamic exchange of S–S bonds within the molecular chains, thereby enabling UV-assisted self-healing of the elastomer.[52] It is necessary to point out that, the frictional damage caused by mechanical motion on the surface of elastomer films is generally much smaller than the scratches introduced in the scratch test above. Therefore, the required self-healing time in real-world applications is expected to be shorter than the self-healing time observed here in this work, manifesting that the elastomer has great potential in achieving rapid self-healing of scratches or damages in practical use. The infrared thermal images of the elastomer PUSE under UV irradiation and in a 70 °C oven are shown in the Fig. S8. Under UV irradiation, the surface temperature of the elastomer increased, reaching a maximum average temperature of 46.6 °C after 60 min of irradiation. In contrast, the surface temperature of the elastomer can reach a maximum of 68.4 °C under 70 °C heating. Notably, the temperature rise induced by UV irradiation is much lower than that in 70 °C oven. However, the self-healing efficiency of the elastomer under UV irradiation is higher than that observed under the 70 °C thermal condition. This finding confirms that UV irradiation not only induces photo-thermal heating but also promotes epoxy ring-opening reactions, which assist the self-healing process. Together with thermal activation, these effects establish a photo-thermal synergistic self-healing system.

As shown in Fig. 4d and S9, the surfaces of the PUE and PUS_3E elastomers exhibit hydrophobicity. Upon incorporation of TEC, the water contact angle of the elastomer surface increased from 92° to above 103°. This can be attributed to the presence of methyl groups in TEC, which increases the hydrophobic component in the main chain. After the introduction of APDS, the water contact angle of the elastomer surface decreases slightly but remains above 100°. Fig. 4e also presents macroscopic photographs of the PUE and PUS_3E elastomer. Due to the presence of S–S bonds in PUS_3E, the elastomer appears light yellow compared to the colorless PUE, while still maintaining good optical transparency, the transmittance at 550 nm is 90.55%.

2.4. Preparation and electrical properties of composite conductive elastomer films PUS_3E/AgNWs

Owing to the favorable mechanical properties and self-healing capabilities, PUS_3E could be applied for making flexible strain sensors. Fig. S10 illustrates the preparation process of the composite conductive elastomer PUS_3E/AgNWs. AgNWs were deposited onto glass substrate *via* wire bar coating method, followed by drying at 160 °C. Subsequently, the PUS_3E elastomer precursor sol was uniformly drop-cast onto the surface of AgNWs. After curing at room temperature for 30 min, the composite was peeled off from the glass substrate to obtain the target conductive elastomer film. Fig. S11a shows the sheet resistance of AgNWs films with varying numbers of coating layers. The sheet resistance of the AgNWs film decreased with increasing coating layers, thus AgNWs films with five coating layers was chosen for the following experiments below, which the sheet resistance was as low as 10 Ω sq^{-1}. SEM images of the PUS_3E/AgNWs and PUE/AgNWs films are presented in the Fig. 5a. As observed, a large number of AgNWs are exposed on the surface of the PUS_3E/AgNWs film, and the AgNWs overlap with each other to form a continuous conductive network. In contrast, on the surface of the PUE/AgNWs film, a large portion of AgNWs were encapsulated by the PUE precursor sol, preventing the formation of an effective conductive network of the PUE/AgNWs film, giving rise to the rapid degradation of electrical conductivity with the sheet resistance rises sharply from 10.8 Ω sq^{-1} to 121.4 Ω sq^{-1}. By contrast, the sheet resistance of the AgNWs increased slightly from 11.2 Ω sq^{-1} to 11.6 Ω sq^{-1} after combination with PUS_3E, as displayed in Fig. S11b.

Fig. 5b presents the change in sheet resistance of AgNWs films with different initial resistances before and after being composited with PUS_3E. The change in sheet resistance became larger after transferring with the higher original sheet resistance of the AgNWs film. After bending at a bending radius of 2 cm for 2000 cycles, films with lower initial resistance also exhibited smaller resistance changes (Fig. 5c). Specifically, PUS_3E/AgNWs film with an initial resistance (R_0) of 11.9 Ω increased by only 3.36% after 2000 cycles bending, which was ascribed to the more stable and durable conductive films made up with denser AgNWs network at the surface. In comparison, PUS_3E/AgNWs film with an initial resistance of 62.2 Ω showed 9.16% of increase due to the looser nanowires distribution. Satisfyingly, when the initial resistance of PUS_3E/AgNWs films increased from 11.9 Ω to 62.2 Ω, the corresponding resistance fluctuated within 10% after bending. Exhibiting favorable mechanical stability and presenting great potential in strain–stress sensors. SEM images (Fig. 5d) confirmed that the surface AgNWs network showed no significant cracks or damage after 2000 bending cycles, in accordance with the minimal resistance fluctuation above. However, after 4000 cycles, the AgNWs network suffered notable mechanical degradation with partial nanowire breakage and detachment occurring at the crease regions, resulting in reduced electrical conductivity.

Fig. 5e illustrates the temperature variation of the PUS_3E/AgNWs film under gradually increasing voltage. As shown in

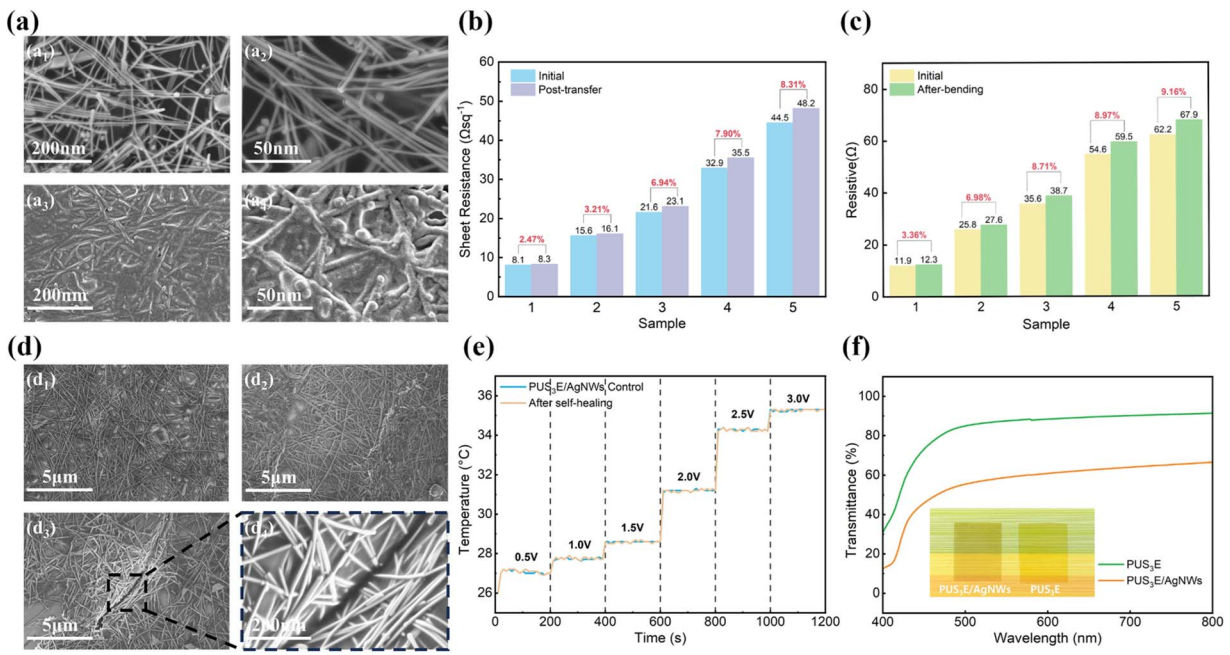

Fig. 5 (a) SEM images of the surface of the elastomer/AgNWs composite conductive film (a_1: PUS_3E/AgNWs 50.0 K, a_2: PUS_3E/AgNWs 200.0 K, a_3: PUE/AgNWs 50.0 K, a_4: PUE/AgNWs 200.0 K). (b) Variation of sheet resistance before and after compositing AgNWs with the PUS_3E elastomer. (c) Variation in sheet resistance of composite conductive films with different sheet resistances before and after 2000 bending cycles. (d) SEM images of the surface of the PUS_3E/AgNWs composite conductive film before and after bending (d_1: 0 cycle 2.0 K, d_2: 2000 cycles 2.0 K, d_3: 4000 cycles 2.0 K, d_4: 4000 cycles 50.0 K). (e) Electrothermal characteristics curve of the PUS_3E/AgNWs composite conductive film under 0–3 V voltage before and after self-healing. (f) Transmittance of the PUS_3E elastomer film before and after compositing with AgNWs in the 400–800 nm range.

the figure, when the voltage remains constant, the surface temperature of the conductive film stabilizes within 200 s, forming a relatively steady thermal plateau, indicating that the PUS_3E/AgNWs film possesses stable electrothermal characteristics. When the voltage increases from 0 V to 3 V, the surface temperature of the PUS_3E/AgNWs film rises from 26 °C to 36 °C. This temperature range falls within the tolerance of human skin, suggesting that the PUS_3E/AgNWs film is suitable for stress–strain sensors in wearable electronics. Furthermore, the overlap of the electrothermal characteristic curves of the PUS_3E/AgNWs film before and after self-healing indicates that the resistance variation on the surface after self-healing in the damaged area is minimal, thus exerting little impact on its electrothermal performance. The visible light transmittance of PUS_3E elastomer film was 87.50% at 550 nm. After the incorporation of AgNWs, the transmittance of the elastomer decreases to 60.42% (seen from Fig. 5f).

2.5. Stress–strain sensor based on PUS_3E/AgNWs

According to the favourable mechanical and electrical stability disscussed above, we constructed a simple stress–strain sensor composed of PUS_3E and AgNWs as flexible support and conductive fillers, individually. Copper tape is attached onto the surface of PUS_3E/AgNWs film and connected to the electrochemical workstation. The PUS_3E/AgNWs wearable strain sensor is capable of monitoring movements across various body parts, such as finger joints, wrist joints, and knee joints during flexion. Fig. 6a illustrates the resistance variation curve associated with elbow flexion. As the elbow bends, the PUS_3E/AgNWs strain sensor undergoes tensile deformation, resulting in an instantaneous increase in resistance. When the arm returns to a relaxed state, the electrical signal quickly recovers. After multiple cycles, the relative change in resistance remains consistent, indicating that the strain sensor possesses excellent stability. In addition to detecting large-scale joint movements, the sensor can also capture subtle vibrations, such as those generated by arterial pulse points. Fig. 6b (Fig. S12) presents the resistance response corresponding to wrist pulse signals. By counting the number of signal peaks, the pulse rate per minute can be calculated, thereby enabling real-time health monitoring. This highlights the sensor's potential applications in the medical field. Flexion tests were also conducted on the finger (Fig. 6c) and knee joint (Fig. 6d). Due to the small-scale of human motion experienced by the sensor during finger bending and wrist pulse compared to that of the elbow and knee joints, the resulting resistance signal change is also small. Since the movement pattern of the knee joint is similar to that of the elbow, their resistance variation amplitudes are comparably aligned. At varying flexion frequencies, aside from differences in vibration frequency, the resistance signal curves remain nearly identical, demonstrating the capability of stable and reliable monitoring of human joint motion. Furthermore, to simulate mechanical damage that may occur in real-world applications, scratches were intentionally introduced on the surface of the PUS_3E/AgNWs sensor (Fig. 6e). After self-healing, repeated experiments involving elbow, finger, and knee flexion as well as pulse monitoring were performed. The electrical signal curves before and after healing exhibit high degrees of overlap, confirming that the self-healing PUS_3E/AgNWs strain sensor shows great potential application in wearable electronic devices. Fig. 6f presents properties comparison between the elastomer developed in this work and previously reported PDMS-based elastomers used in strain sensor applications.[53–55] The PUS_3E/AgNWs elastomer exhibits a pronounced advantage in optical transparency while achieving a favorable balance between tensile strength and self-healing efficiency. Besides, an additional Table S1 was summarized, emphasizing on the mechanical performance advantages of the elastomer in this work.

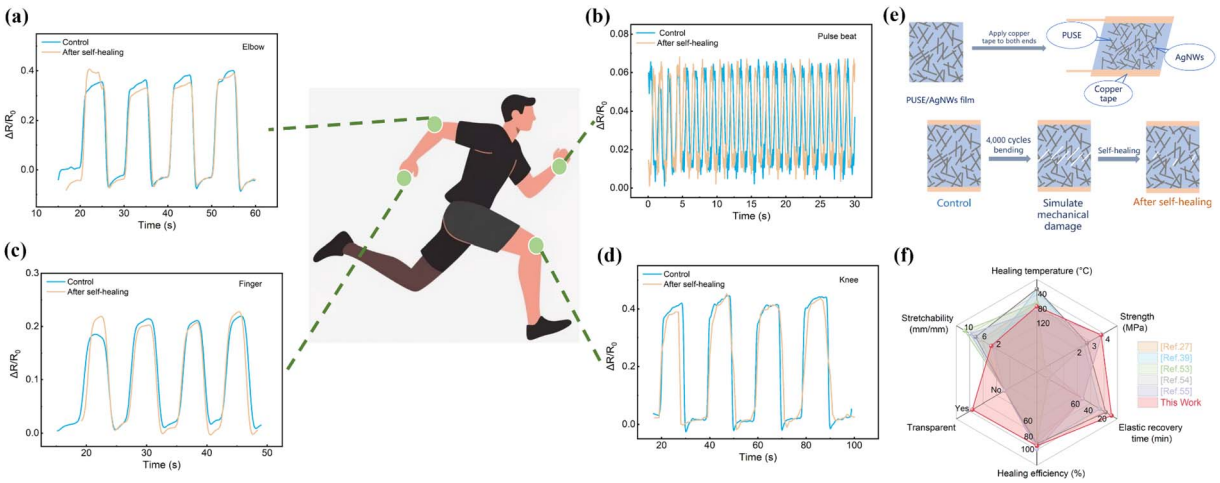

Fig. 6 (a) Elbow joint signal monitoring of PUS_3E/AgNWs strain sensors. (b) Pulse beat signal monitoring of PUS_3E/AgNWs strain sensors. (c) Finger joint signal monitoring of PUS_3E/AgNWs strain sensors. (d) Knee joints signal monitoring of PUS_3E/AgNWs strain sensors. (e) Fabrication process of a PUS_3E/AgNW-Based strain sensor and illustration of the damage and self-healing behavior. (f) Comparison of elastomers in the performance of tensile strength, stretchability, self-healing efficiency, healing temperature, elastic recovery, and transparency of this work with previously reported self-healing polymers.

3 Conclusion

In summary, a self-healing polydimethylsiloxane (PDMS) elastomer, PUS_3E, with excellent mechanical properties and photothermal responsiveness was designed and synthesized in this study, and the structure–property relationships between its molecular design, mechanical performance, and self-healing behavior were systematically investigated. By incorporating the planar cyclic structure of TEC and the aromatic structure of APDS, the mechanical strength of the elastomer was significantly enhanced, achieving a tensile strength of up to 4.2 MPa. The epoxy groups in TEC and the disulfide bonds in APDS imparted responsiveness to ultraviolet (UV) light, enabling a self-healing process that is primarily thermally driven and secondarily UV-assisted, with a healing efficiency of 94.76% within 24 h. Furthermore, a PUS_3E/AgNWs conductive elastomer composite was successfully fabricated *via* a transfer-printing method. The PUS_3E/AgNWs composite exhibited excellent mechanical stability and visible-light transmittance, along with stable electrical signal responses to human motions such as finger bending, wrist bending, knee bending, and pulse detection. Overall, the light- and heat-responsive PUS_3E elastomer not only provides an effective strategy to balance mechanical strength and self-healing capability but also shows potential for applications in wearable electronic devices.

4 Experimental section

4.1. Materials

Amino-capped polydimethylsiloxane (PDMS, Mw: 3000) was purchased from Shanghai Macklin Biochemical Co., Ltd; isophorone diisocyanate (IPDI, 99%), 4, 4′-dithiodianiline (DTSA, 98%) was bought from Anhui Senrise Technologies Co., Ltd; 2, 4, 6, 8 – tetramethyl – 2, 4, 6, 8 – tetrakis [3-(oxiranylmethoxy) propyl] cyclotetrasiloxan (TEC, 97%) were provided from Zhengzhou Alfa Chemical Co., Ltd; tetrahydrofuran (THF), silver nanowires (AgNWs), and Dibutyltindilaurate were purchased from Shanghai Aladdin Biochemical Technology Co., Ltd; all of the reagents can be used without purification.

4.2. Preparation of PUSE elastomer

A total of 2 mmol of H_2N-PDMS-NH_2 was dispersed in 20 mL of THF. Subsequently, 4 mmol of IPDI was dissolved in 10 mL of THF, and the resulting solution was added to the PDMS dispersion. Under a nitrogen atmosphere, the diluted H_2N–PDMS–NH_2 solution was transferred into a 100 mL two-neck flask using a disposable syringe. The mixture was stirred at room temperature for 10 min and then heated to 60 °C. The diluted IPDI solution and 4, 4′-dithiodiphenylamine (dissolved in THF) were then slowly injected into the flask *via* syringe. The reaction mixture was maintained at 60 °C with continuous stirring for 24 h to yield the PDMS-PUS composite sol. Subsequently, TEC (1 wt% relative to the total mass of PDMS and IPDI) was dissolved in 5 mL of THF and added dropwise to the PUS sol together with dibutyltin dilaurate. The mixture was further reacted at 60 °C under 365 nm UV irradiation for 6 h to obtain the PUSE sol. The PUSE sol was poured into a mold and cured under UV light for 12 h, followed by additional curing in a vacuum oven at 60 °C for 12 h to obtain the final PUSE elastomer.

4.3. Preparation of PUSE/AgNWs elastomer

First, AgNWs films were fabricated on 4 × 7 cm glass substrates *via* a roll-coating process, yielding a film thickness of approximately 30 nm and a sheet resistance below 10 Ω sq^{-1}. The sheet resistance was regulated by adjusting the AgNWs dispersion concentration, the roll-coating speed, and the number of coating cycles. The coated AgNWs films were then annealed in an oven at 160 °C for 30 min to reduce the junction resistance. Subsequently, the PUS_3E precursor solution was drop-cast onto the AgNWs films and cured under irradiation from a 365 nm, 80 W UV lamp. After solvent evaporation, the cured film was peeled from the glass substrate to obtain the PUS_3E/AgNWs elastomer. Finally, copper tape was attached to both edges of the composite elastomer to form simple electrodes for subsequent electrical testing.

4.4. Characterization

The ^{1}HNMR spectrum was recorded on a Bruker AVANCE III 400 MHz spectrometer. FTIR spectra were obtained using a Thermo Fisher Nicolet 6700 instrument. X-ray photoelectron spectroscopy (XPS) measurements were carried out on a Kratos AXIS SUPRA system. Raman spectra were collected using a Renishaw inVia Reflex spectrometer. Thermogravimetric analysis (TGA) was performed on a TG209F1 analyzer under an argon atmosphere, and differential scanning calorimetry (DSC) measurements were conducted using a DSC214 instrument. Optical images were captured using a TD-TZG5X-KHT industrial digital microscope at a magnification of 10×. Scanning electron microscopy (SEM) images were recorded using a Kratos AXIS SUPRA system.

The tensile properties were evaluated following the GB/T 528–2009 (China) standard using a universal testing machine equipped with a 1 kN load cell. For electrothermal characterization, the PUSE/AgNW conductive elastomer was powered by a DC voltage source. The surface temperature variation under applied voltages ranging from 0.5 V to 3.0 V was monitored using an infrared thermometer. An electrochemical workstation was employed to monitor the electrical signal responses induced by human motion.

Surface scratch experiments were conducted on elastomers by applying scratches on the surface using a hobby knife. The recovery of surface scratches was observed through an optical microscope after repairing under various conditions. The original dumbbell-shaped samples were halved at the center, and the separated samples were repaired under different conditions: a 70 °C oven, and a 365 nm, 80 W UV lamp for 24 h. Subsequently, their tensile strengths were tested using a universal material testing machine, and the ratio of the maximum stresses of the repaired samples to the initial samples was used to calculate the self-healing efficiency of the elastomers:

$$\text{Self-healing efficiency} = \frac{\sigma_m}{\sigma_0} \times 100\% \quad (1)$$

σ_0: the maximum stress of the initial sample, σ_m: the maximum stress of the healed sample.

Toughness (W) is defined as the area surrounded by the engineering stress (σ)–strain (ε) curves and is calculated by the following equation:

$$W = \int_{\varepsilon=0}^{\varepsilon=\varepsilon_{max}} \sigma \, d\varepsilon \quad (2)$$

PUS_3E/AgNWs conductive elastomers were subjected to an external voltage using a DC power supply. The surface temperature change was then measured using an infrared thermometer gun for voltages ranging from 0 V to 3 V.

Copper tape was applied to both ends of the PUS_3E/AgNWs conductive elastomers to form a simple strain transducer, which was tightly fitted to the finger joints, wrist joints, and pulses, and an electrochemical workstation was used to test the changes in the elastomer resistance during different motions.

Ethical statement

Informed consent was obtained for all experiments involving human volunteers.

Author contributions

Ruijie Zhu: writing – review & editing, writing – original draft, visualization, validation, methodology, investigation, formal analysis, data curation. Zhou Zhou: visualization, methodology, investigation. Jie Gao: methodology, data curation. Yuanlong Zhong: methodology, data curation. Qi Zhang: visualization, methodology. Ling Ai: writing – review & editing, visualization, supervision, resources, funding acquisition, conceptualization. Weijie Song: resources, funding acquisition, conceptualization.

Conflicts of interest

The authors declare that they have no conflicts of interest.

Data availability

Additional data used for the study are available from the corresponding authors upon reasonable request.

The authors declare that all data supporting the results reported in this study are available within the paper and the supplementary information (SI). Supplementary information is available. See DOI: https://doi.org/10.1039/d6ra01474g.

Acknowledgements

This work was financially supported by the the National Key R&D Program of China (2023YFC3011602) and and Jiangsu Province Cultivation Base for State Key Laboratory of Photovoltaic Science and Technology.

References

1 X. Y. Yu, H. Li and J. W. Wang, Recent advances and future prospects of wearable sensors based on nanomaterial sensing mechanisms for biosafety monitoring, *Chem. Eng. J.*, 2025, **512**, 1385–8947.
2 A. Ajeev, T. Warfle and S. Maslaczynska-Salome, From the synthesis of wearable polymer sensors to their potential for reuse and ultimate fate, *Chem. Sci.*, 2025, **16**, 9056–9075.
3 S. Pal, D. Kumar and F. Ulucan-Karnak, Bio-inspired electronic sensors for healthcare applications, *Chem. Eng. J.*, 2024, **499**, 1385–8947.
4 H. J. Li, L. Long and H. Zhang, Cell differentiation-inspired, salt-induced multifunctional gels for an intelligent soft robot with an artificial reflex arc, *ACS Appl. Mater. Interfaces*, 2023, **15**, 5910–5920.
5 M. Yang, K. L. Peng and Z. Li, Recent progress in flexible materials for wearable devices for body function and athletic performance monitoring, *Chem. Eng. J.*, 2025, **505**, 1385–8947.
6 C. Y. Huang, X. H. Jia and D. Wang, Stretchable ionogels: Recent advances in design, toughening mechanisms, material properties and wearable devices applications, *Chem. Eng. J.*, 2024, **490**, 1385–8947.
7 Z. Jiang, N. Chen and Z. Yi, 1.3-micrometre-thick elastic conductor for seamless on-skin and implantable sensors, *Nat. Electron.*, 2022, **5**, 784–793.
8 Y. Zhu, Y. He, W. Lu, H. Tian, F. Fei, P. Zhou and J. Wang, Multi-functional self-healing polyurethane elastomer based on chair conformation for strain sensors, *J. Mater. Chem. A*, 2024, **12**, 28716.
9 W. Wang, H. X. Lin and Y. L. Huang, Intelligent conductive gels for advanced flexible electronics, *Chem. Eng. J.*, 2024, **500**, 1385–8947.
10 J. Liu, Y. Yao and X. H. Li, Fabrication of advanced polydimethylsiloxane-based functional materials: Bulk modifications and surface functionalizations, *Chem. Eng. J.*, 2021, **408**, 1385–8947.
11 T. Liu, T. Wang and S. Zhang, Recent advancements in wearable self-healing polysiloxane materials and wearable sensors, *Wearable Electron.*, 2025, **2**, 40–54.
12 Z. P. Yang, H. Q. Li and C. K. Li, Conductive and room-temperature self-healable polydimethylsiloxane-based elastomer film with ridge-like microstructure for piezoresistive pressure sensor, *Chem. Eng. J.*, 2022, **430**, 1385–8947.
13 L. Li, Y. Zheng, E. Liu and Y. Chen, Ultrafast dynamic response of waterproof stretchable strain sensors based on wrinkle-templated microcracking, *J. Mater. Chem. A*, 2022, **10**, 16297–16308.
14 X. Chen, Y. Zhang, H. Wang and Z. Liu, A double-crack structure for bionic wearable strain sensors with ultra-high sensitivity and a wide sensing range, *Nanoscale*, 2024, **16**, 5891–5902.
15 F. Sun, L. Liu, T. Liu and X. Wang, Vascular smooth muscle-inspired architecture enables soft yet tough self-healing

materials for durable capacitive strain-sensor, *Nat. Commun.*, 2023, **14**, 130.
16 M. Qi, R. Yang and Z. Wang, Bioinspired self-healing soft electronics, *Adv. Funct. Mater.*, 2023, **33**, 2214479.
17 E. K. Boahen, B. Pan, H. Kweon, *et al.*, Ultrafast, autonomous self-healable iontronic skin exhibiting piezo-ionic dynamics, *Nat. Commun.*, 2022, **13**, 7699.
18 J. Tu, H. Xu and G. F. Xiang, Rapid self-healing and tough polyurethane based on the synergy of multi-level hydrogen and disulfide bonds for healing propellant microcracks, *Mater. Chem. Front.*, 2022, **6**, 1161–1171.
19 H. Dong, X. Yang and W. J. Huang, High strength, recyclable, durable polydimethylsiloxanes based on carboxylic acid aromatic disulfides with highly efficient room-temperature self-healing, *Polymer*, 2025, **320**, 128125.
20 T. Zhang, Y. T. Shi and W. Y. Chen, Spider silk-inspired supramolecular polydimethylsiloxane network with prominent mechanical robustness for bifunctional flexible electronics, *Eur. Polym. J.*, 2024, **213**, 113–122.
21 X. H. Liu, E. D. Zhang and J. M. Liu, Self-healing, reprocessable, degradable, thermadapt shape memory multifunctional polymers based on dynamic imine bonds and their application in nondestructively recyclable carbon fiber composites, *Chem. Eng. J.*, 2023, **454**, 139992.
22 F. B. Luo, J. Y. Sun and Y. B. Zou, Outstanding self-healing and plasticity of imine-linked dynamic PDMS with high softness and stability, *Chem. Eng. J.*, 2025, **511**, 161905.
23 X. Y. Zhu, B. Huang and L. N. Dong, Rheology, dynamics, and mechanisms of self-healing of polydimethylsiloxane dual-linked by ureido and dynamic imine bonds, *J. Colloid Interface Sci.*, 2025, **700**, 138512.
24 Z. Zhang, J. He, Z. He, *et al.*, Sustainable fabrication of metal-ligand coordinated self-healing conductive organosilicon elastomers for flexible sensor applications, *Microchem. J.*, 2025, 116368.
25 S. C. Liu, Y. T. Li and Y. Q. Qin, Mechanically strong, stretchable and self-healable silicone elastomers with designed dynamic networks for exceptional self-adhesion under harsh conditions, *Adv. Ind. Eng. Polym. Res.*, 2025, **8**, 422–432.
26 J. H. Mo, W. J. Wu and S. J. Shan, A systematic study on Zn(II)-Iminocarboxyl complexation applied in supramolecular PDMS networks, *Polymer*, 2022, **250**, 124896.
27 H. T. Zhu, H. Lu and J. H. Xu, Tough and self-healing linear polydimethylsiloxane elastomer with multiple hydrogen bonds for high-performance piezoresistive pressure sensor, *Appl. Mater. Today*, 2024, **40**, 102411.
28 S. Z. Yue, Y. Z. Liu and Z. Y. Tian, Self-powered and integral self-healing dielectric elastomer actuator with a robust interface, *Nano Energy*, 2025, **139**, 110974.
29 W. Zheng, C. S. Zhang and Y. J. Han, Highly Durable Silicone-Based Elastomers Achieved Through the Synergy of Bi-Incompatible Soft Segments and Multi-Scale Hydrogen Bonds, *Small*, 2024, **20**, 2402124.
30 J. Yang, P. R. Cao and Q. Dou, Synergistic enhancement of low-temperature strength and toughness in poly (boron-urethane) elastomers *via* π-π stacking and hydrogen bonding, *Chem. Eng. J.*, 2025, **503**, 158459.
31 Y. M. Kim, K. S. Yu and H. C. Moon, Regulating the π–π interactions of copolymer gelators: Effective molecular design of highly stretchable and tough ionogels for wearable ionotronics, *Chem. Eng. J.*, 2024, **480**, 147947.
32 S. Gaikwad and M. W. Urban, Ring-and-Lock Interactions in Self-Healable Styrenic Copolymers, *J. Am. Chem. Soc.*, 2023, **145**, 9693–9699.
33 S. Kim, J. W. Kim and Y. H. Lee, Tough, self-healing polyurethane with novel functionality for fully recoverable layered sensor arrays, *Chem. Eng. J.*, 2023, **464**, 142700.
34 C. W. Lin, C. Y. Liang and J. D. Li, Transparent, Tough, and Self-Healable Elastomer Based on Dynamic Dual Cross-Linking of Coordination and Disulfide Bonds, *ACS Appl. Polym. Mater.*, 2024, **6**, 4516–4524.
35 W. X. Liu, D. Liu, Y. Xiao, *et al.*, Healable, Recyclable, and High-Stretchable Polydimethylsiloxane Elastomer Based on Synergistic Effects of Multiple Supramolecular Interactions, *Macromol. Mater. Eng.*, 2022, **307**(10), 2200310.
36 K. Y. Lam, C. S. Lee and M. R. Pichika, Light-responsive polyurethanes: classification of light-responsive moieties, light-responsive reactions, and their applications, *RSC Adv.*, 2022, **12**, 15261–15283.
37 X. W. Xu, X. Y. Hao and J. Hu, Recyclable silicone elastic light-triggered actuator with a reconfigurable Janus structure and self-healable performance, *Polym. Chem.*, 2022, **6**, 829–837.
38 C. Deng, Y. Lin, X. Ge, *et al.*, Facile synthesis of carbon dioxide and UV light dual-responsive asymmetric tetrablock polymers[J]. Reactive and Functional, *Polymers*, 2024, **205**, 106077.
39 X. R. Shi, K. Y. Zhang and J. X. Chen, Octopi Tentacles-Inspired Architecture Enables Self-Healing Conductive Rapid-Photo-Responsive Materials for Soft Multifunctional, *Adv. Funct. Mater.*, 2024, **34**, 2311567.
40 L. Li, Z. P. Zhang and M. H. Wang, UV-curable epoxy acrylate composite coatings with high flexibility, super-hydrophobicity, wear-resistance and self-healing property, *Prog. Org. Coat.*, 2023, **182**, 107649.
41 B. W. Peng, H. Li and Y. T. Li, A photoresponsive azopyridine-based supramolecular elastomer for self-healing strain sensors, *Chem. Eng. J.*, 2020, **395**, 125079.
42 J. F. Fan, W. J. Wu and X. L. Zeng, Dual Reversible Network Nanoarchitectonics for Ultrafast Light-Controlled Healable and Tough Polydimethylsiloxane-Based Composite Elastomers, *ACS Appl. Mater. Interfaces*, 2023, **15**, 38996–39007.
43 B. Jiang, X. R. Shi and T. Zhang, Recent advances in UV/thermal curing silicone polymers, *Chem. Eng. J.*, 2022, **435**, 134843.
44 L. W. Zhao, Y. Yin and B. Jiang, Fast room-temperature self-healing siloxane elastomer for healable stretchable electronics, *J. Colloid Interface Sci.*, 2020, **573**, 105–114.
45 Z. Q. Pan, M. F. Chen and K. L. Zeng, Synthesis and application of cyclotetrasiloxane modified with epoxy resins, *Polym. Bull.*, 2022, **79**, 7177–7192.

46 L. Wang, Y. B. Cai and H. R. Zhang, Room-temperature self-healing polysiloxane elastomer with reversible cross-linked network, *Polymer*, 2022, **256**, 125272.
47 H. S. Guo, Y. Han and W. Q. Zhao, Universally autonomous self-healing elastomer with high stretchability, *Nat. Commun.*, 2020, **11**, 2037.
48 S. Z. Yue, Y. Z. Liu and Z. Y. Tian, Self-powered and integral self-healing dielectric elastomer actuator with a robust interface, *Nano Energy*, 2025, **139**, 110974.
49 Z. Wang, Y. T. Liu and D. J. Zhang, Mussel-inspired self-healing PDMS/AgNPs conductive elastomer with tunable mechanical properties and efficient antibacterial performances for wearable sensor, *Compos. Part B: Eng.*, 2021, **224**, 109213.
50 K. M. Zhang, Z. Wang and J. H. Zhang, A highly stretchable and room temperature autonomous self-healing supramolecular organosilicon elastomer with hyperbranched structure, *Eur. Polym. J.*, 2021, **156**, 110618.
51 M. F. Li, Q. Q. Li and W. W. Wang, Tough and self-healing polyurethane elastomer and its application for fiber-based self-encapsulating strain sensor, *Chem. Eng. J.*, 2025, **513**, 162791.
52 D.-H. Qu, Y. Deng and Z. Huang, Converting inorganic sulfur into degradable thermoplastics and adhesives by copolymerization with cyclic disulfides, *Nat. Commun.*, 2024, **15**, 5632.
53 T. Zhang, *et al.*, Synergistic Self-Healing Enhancement in Multifunctional Silicone Elastomers, *Polymers*, 2024, **16**, 487.
54 P. Y. Lai, Y. Yuan, Y. W. Huang, *et al.*, Preparation of Robust, Room-Temperature Self-Healable and Recyclable Polysiloxanes Based on Hierarchical Hard Domains, *Adv. Eng. Mater.*, 2023, **25**, 2300129.
55 W. Y. Zeng, L. J. Deng and G. Yang, Self-Healable Elastomeric Network with Dynamic Disulfide, Imine, and Hydrogen Bonds for Flexible Strain Sensor, *Chem.–Eur. J.*, 2023, **29**, e202203478.